Electrochimica Acta 439 (2023) 141701

Contents lists available at ScienceDirect

Electrochimica Acta

journal homepage: www.journals.elsevier.com/electrochimica-acta

α-$FAPbI_3$ powder presynthesized by microwave irradiation for photovoltaic applications

Omar E. Solis [a,b,c], Carolina Fernández-Saiz [c], Jesús Manuel Rivas [a], Diego Esparza [a], Silver-Hamill Turren-Cruz [c,*], Beatriz Julián-López [c,*], Pablo P. Boix [b], Iván Mora-Seró [c,*]

[a] Unidad Académica de Ingeniería Eléctrica, Universidad Autónoma de Zacatecas, Av. Ramon López Velarde 801, Col. Centro, Zacatecas, Zac. 98060, México
[b] Instituto de Ciencia de los Materiales de la Universidad de Valencia (ICMUV), Paterna, Valencia 46980, Spain
[c] Institute of Advanced Materials (INAM), University Jaume I, Av. Vicent Sos Baynat, s/n, Castellón de la Plana 12071, Spain

ARTICLE INFO

Keywords:
Perovskite
$FAPbI_3$
Presynthesized powder
Microwave synthesis
Solar cells
Photovoltaics

ABSTRACT

The development of up-scalable and high-throughput methodologies to fabricate high-efficiency lead halide perovskite solar cells (PSCs) based on α-phase formamidinium lead iodide ($FAPbI_3$) is one of the main challenges of making solar energy economical. In this context, PSCs based on α-phase formamidinium lead iodide ($FAPbI_3$) are receiving special attention as this perovskite has the highest theoretical photoconversion efficiency (PCE). This manuscript reports an easy, fast and environmentally-friendly way to prepare α-$FAPbI_3$ black powders by a microwave-assisted synthesis and their application in solar cells. The α-$FAPbI_3$ powders consist of micrometric particles that can be stored for weeks in a closed vial at ambient conditions. This technique presents an enormous potential for upscaling $FAPbI_3$ powders synthesis prerequisite necessary for large scale commercialization. The performance of the presynthesized $FAPbI_3$-based solar cell was comparable with that of PSCs fabricated with the conventional procedure from precursors solutions, leading to a maximum PCE value of 18.15%, with an V_{OC}=1.07 V, a J_{sc}=24.28 mA/cm^2 and an FF=70%. The presynthesized $FAPbI_3$-based solar cell was further modified through the addition of methylammonium chloride (MACl) in order to study the generality of the approach. The optical band gap for the presynthesized perovskite shifted from ~1.43 eV to ~1.55 eV with the MACl addition (30 mol%), indicating the formation of a mixed methylammonium and formamidinium based perovskite material ($MAFAPbI_3$). In addition, the incorporation of MACl led to an increase in the grain size and the disappearance of the residual δ-phase perovskite, thus improving the efficiency of the final device.

1. Introduction

Recently, halide perovskites have emerged as a very promising class of materials for thin film photovoltaics due to their high-power photovoltaic conversion efficiency (PCE) in solar cells 25.7% [1] and the outstanding optical and electrical properties [1–4], despite the polycrystalline nature of the thin films. Among them, formamidinium lead triiodide ($(HC(NH_2)_2PbI_3$ or $FAPbI_3$) in the black cubic perovskite phase presents the lowest band gap ~1.43 eV [5,6], extending the absorption into the near-infrared, with a bandgap close to ideal one considering the Schockley–Queisser limit. However, at room temperature the black phase, also known as α- phase, of $FAPbI_3$ evolves towards the most stable non-perovskite hexagonal yellow δ-phase (δ-$FAPbI_3$) [7,8] because α-$FAPbI_3$ is thermodynamically unstable at temperatures below 150 °C [9]. To prevent the undesired evolution, the formamidinium-based perovskite is combined with smalls cations like methylammonium (MA), cesium (Cs) and rubidium (Rb) or with biggest organic cations (2D/3D cations) [10–15]. The addition of different cations, produces more stable perovskites with higher efficiency but widening the band gap, [16,17] and consequently reducing the maximum theoretical PCE that can be reached.

On the other hand, spin-coating deposition of the halide perovskite from the perovskite precursors solution is the conventional way to deposit perovskite thin films for the fabrication of solar cells, either by the one-step anti-solvent method [18–20] or by the two-step method [21–23]. However, more recently, another approach to prepare perovskite solar cells has been proposed, which consist of presynthesizing the $FAPbI_3$ perovskite as a powder and dissolving it for direct deposition. Different ways of presynthesizing the perovskite powders have been reported, these methods provide higher material purity, major

* Corresponding authors.
E-mail addresses: turren@uji.es (S.-H. Turren-Cruz), julian@uji.es (B. Julián-López), sero@uji.es (I. Mora-Seró).

https://doi.org/10.1016/j.electacta.2022.141701
Received 29 June 2022; Received in revised form 13 October 2022; Accepted 9 December 2022
Available online 10 December 2022

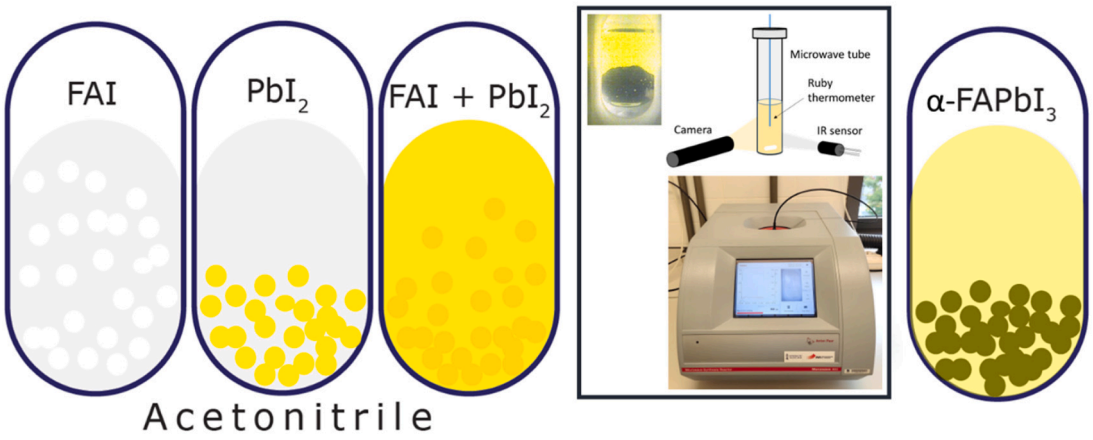

Fig. 1. Schematic diagram of $FAPbI_3$ powder synthesis assisted by microwave radiation.

reproducibility and better stoichiometry [24–26]. This presynthesis purifies the initial precursors and help to increase device performance. Nevertheless, the presynthesis of the perovskite powder could constitute a bottleneck in the fabrication process. Consequently, the development of a presynthesis process that can be easily scaled up is a prerequisite for the full commercial exploitation of this approach. In this work, we present the synthesis of the α-$FAPbI_3$ powders by a fast and easy microwave-assisted synthesis (MWAS) easily up scalable for the use in perovskite solar cells (PSCs).

2. Experimental section

2.1. Materials

Lead iodide (PbI_2, 99.999%) was purchased from ABCR. Formamidinium iodide (FAI, $HC(NH_2)_2I$, 99.99%) and methylammonium chloride (MACl, 99%) were purchased from Greatcell Solar. Acetonitrile (ACN, anhydrous, 99.8%) for the powder synthesis, dimethyl sulfoxide (DMSO, 98%), dimethyl formamide (DMF, 98%), chlorobenzene (CB, 99%), titanium diisopropoxide bis(acetylacetonate) (97%), acetylacetone (99%), Spiro-MeOTAD (FEIMING CHEMICAL LIMITED), Bis(trifluoromethane)sulfonimide lithium salt (LiTFSI, 99.95%) and 4-tert-Butylpyridine (TBP, 98%) were purchased from Sigma-Aldrich. Titanium dioxide paste (30-NRD from Dye Solar Cells, 99%). All the purchased chemicals were used as received without further purification.

2.2. Microwave-assisted synthesis (MWAS) of $FAPbI_3$ powder

In a general synthesis, 0.5041 g of PbI_2 were loaded into a microwave (MW) glass tube (total volume of 30 mL). Then, 1.6 mL of ACN were added and stirred for 2 min. Separately, 0.2407 g of FAI (1.4 mmol) were dissolved in 5 mL of ACN and added to the previous MW tube. After 5 min of stirring, the tube was placed in the MW reactor and heated at 10 °C/min up to T_{max} (T_{max}: 100 °C, 110 °C, 120 °C or 150 °C) for 2 min. Video S1 in the Supporting Information shows the microwave-assisted reaction. The process is summarized in Fig. 1. The system was left cooling with compressed air. The resulting black powder was decanted out and washed twice with ACN. The $FAPbI_3$ powder was recovered by centrifugation at 5000 rpm for 5 min, followed by oven drying at 120 °C, and kept there until use (at least for 24 h). Fig. S1 shows some photographs of the black MWAS perovskite powders synthesized at different temperatures. After drying at 120 °C for 24 h, the samples are stable in air conditions and can be stored at room temperature in closed vials for at least one month without any degradation or phase transformation.

Reaction temperature was varied from 80 °C to 150 °C, and 120 °C was selected as it was the lowest temperature producing good performance PSCs. Below 80 °C, no reaction between FA and Pb precursors was achieved.

2.3. Device fabrication

FTO substrates (2.5 × 2.5 cm) were washed in an ultrasonic bath during 15 min per process. First, the substrates were washed in water with soap and rinsed with distilled water. Then, the substrates were washed with ethanol, acetone and isopropanol, respectively, and finally dried with N_2. For the deposition of the electron transport material (TiO_2-c) 720 μl of Titanium diisopropoxide bis(acetylacetonate), 480 μl of acetylacetone and 10.8 ml of ethanol were mixed. This solution was deposited by spray pyrolysis at 450 °C with an annealing treatment for 30 min. After cooling, a film of TiO_2-m was deposited by spin coating. The precursor solution was prepared mixing TiO_2 paste with ethanol (6:1 in mass) and stirring 24 h before the deposition. The deposit of this film was performed at 4000 rpm for 10 s. The substrates were heated at 100 °C for 10 min. Finally, an annealing treatment was done at 450 °C for 30 min.

Then, the perovskite films were deposited by spin coating. The precursor solution of the presynthesized $FAPbI_3$ was prepared by dissolving the $FAPbI_3$ powder in a mixture of DMF:DMSO (4:1 in volume) with a molar concentration of 1.24M. For comparison purposes, the conventional procedure (CP) was also employed. In that case, the perovskite conventional solution was prepared by mixing FAI (0.3 g), PbI_2 (0.98 g) and 1.410 ml of a mixture of DMF:DMSO (4:1 in volume).

The perovskite films were deposited using 80 μl of the precursor solution. The speed of the spin coating was 4000 rpm for 30 s. After 25 s, 250 μl of chlorobenzene was deposited like antisolvent. Finally, an annealing treatment was done at 120 °C for 30 min in both methodologies. Fig. S1d shows a picture of the films prepared with the presynthesized $FAPbI_3$ powders. Furthermore, in order to improve the quality of the $FAPbI_3$ films, 30 mol% of MACl was added in the precursor solutions for both procedures (presynthesized powder and one-step precursor solution). Then, the films were prepared in a similar manner. The hole transport material was deposited by spin coating. The precursor solution was prepared mixing Spiro-MeOTAD (0.16 g), chlorobenzene (1.740 ml), 4-tert-Butylpyridine (63 μl) and 36 μl of LiTFSI solution (0.52 g of LiTFSI dissolved in 1 ml of acetonitrile). The Spiro-MeOTAD was deposited using 80 μl of the precursor solution. The speed of the spin coating was 4000 rpm for 30 s. After 1–5 s, after starting the spin coating, the precursor solution is deposited.

Finally, a gold film (80 nm) was deposited, like metallic contact, by thermal evaporation at a rate of 10 Å/s.

3. Results and discussion

$FAPbI_3$ powders obtained by MWAS have been systematically

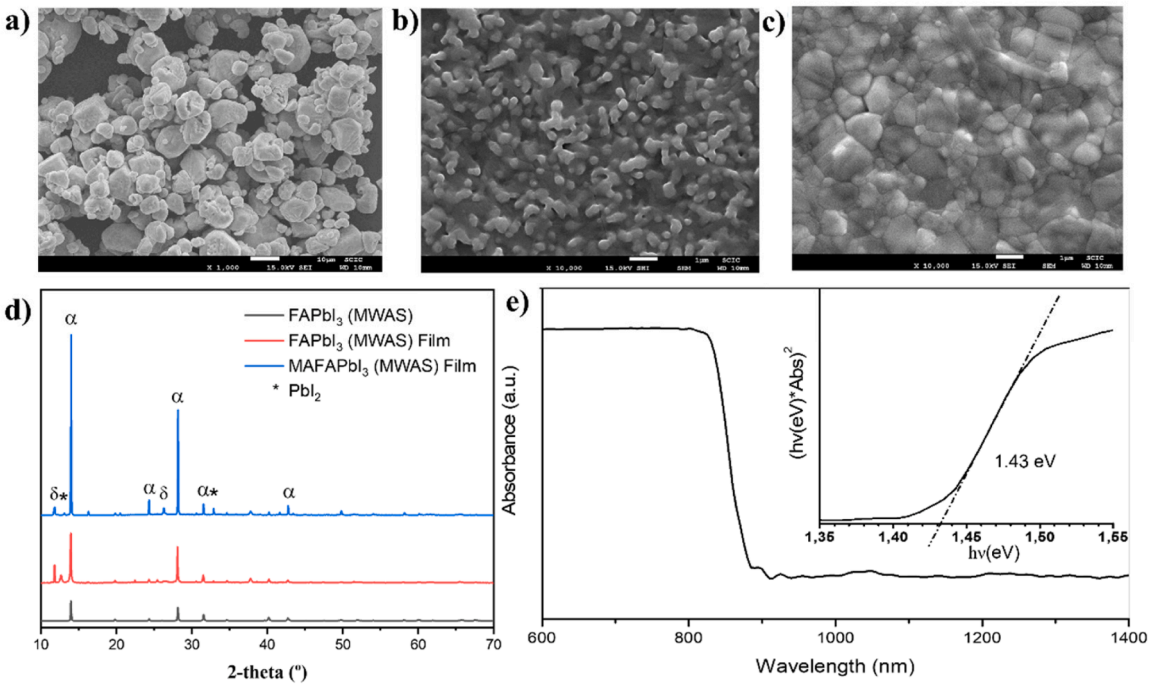

Fig. 2. SEM images of (a) black $FAPbI_3$ phase (the scale bar is 10 μm), (b) perovskite film without MACl (the scale bar is 1 μm), (c) perovskite film with MACl, (the scale bar is 1 μm), (d) XRD patterns of $FAPbI_3$ powders and perovskite films with and without MACl. The α and δ labels in the XRD patterns represents the main peaks of α-phase and δ-phase of the perovskite. and (e) UV-VIS-NIR spectrum with the respective Tauc plot (as inset) of the $FAPbI_3$ black power obtained from MWAS at 120 °C.

characterized. SEM images revealed that the black powder is formed by irregularly shaped particles with sizes ranging from 2 to 10 μm, see Fig. 2a. The XRD pattern of the $FAPbI_3$ powders obtained at 120 °C exhibits the characteristic peaks of the black α-$FAPbI_3$ phase [27], see Fig. 2d (black line). Identical XRD patterns were obtained for powders produced at different MWAS temperatures in the 100–150 °C range, see Fig. S2.

Fig. 2b shows a SEM image of perovskite thin film prepared using MWAS presynthesized $FAPbI_3$ powder. It presents an average grain size of 0.47±0.13 μm. The grain size histogram is included in the Fig. S3a. The XRD pattern of perovskite film, see Fig. 2d, shows that the prepared films exhibit the black α-$FAPbI_3$ phase, [28] as the major phase, but some residual amount of the yellow δ-$FAPbI_3$ phase [29] can be detected. After adding MACl (30 mol%) in the film, the morphology of the surface changes and the grain size increases significantly [30,31] up to an average grain size of 0.84±0.25 μm, see Fig. 2c and see Fig. S3b for the grain size histogram. More interestingly, the XRD pattern, see Fig. 2d, also reveals that the black α-$MAFAPbI_3$ peaks are more prominent upon MACl addition, and a significant decrease of the yellow δ-$MAFAPbI_3$ phase is observed. The addition of MACl in the solution processing of I-based perovskite synthesis has been reported as a method to enhance the systems crystallinity [32,33]. This extent is confirmed by the X-ray diffraction pattern, which show an increase in the peak intensity, pointing to better crystallinity [34,35]. Fig. S4 shows the characteristic perovskite peak (110) for $FAPbI_3$ (13.95°), $MAFAPbI_3$ (14.00°) and $MAPbI_3$ (14.10°) and the characteristic peak (100) for $FAPbCl_3$ (15.41°) and $MAPbCl_3$ (15.52°). A small shift towards higher angles is detected when the MACl is added into the $FAPbI_3$ perovskite solution. This indicates that the MA^+ ions are incorporated into the $FAPbI_3$ structure. In contrast, the Cl^- ions are not incorporated into the $MAFAPbI_3$ perovskite since no new and/or shifted peaks associated to Cl-containing phases are observed. These results agree well with previous reports, [31,36] and this is because the growth of hybrid mixed I/Cl perovskites are energetically unfavorable [31,36]. Thus, Cl^- ions are certainly evaporated during the annealing process [34,37,38].

The UV-Vis-NIR absorption spectrum of the powder, Fig. 2e, shows the absorption onset located in the infrared region. The optical band gap, with a value of 1.43 eV, was determined from Tauc plot graphs, inset in Fig. 2e. This result is in good agreement with that reported in the literature for the black $FAPbI_3$ phase. [27] The samples prepared at different MWAS temperatures display similar band gaps, see in Fig. S2b, slightly varying from 1.42 to 1.44 eV.

The absorption and photoluminescence (PL) spectra for the perovskite films with MACl prepared by MWAS α-$FAPbI_3$ powder and by the conventional procedure (CP), from FAI and PbI_2 solution, are represented in the Fig. 3a, with slightly higher absorption from films prepared by CP. However, the PL signal is higher for the sample fabricated by MWAS, indicating lower non-radiative recombination in the devices fabricated by MWAS than for devices fabricated by the CP [39]. The optical band gaps were determined from Tauc Plot, see Fig. 3b, leading to values of ~1.55 eV for both methods. Consequently, the addition of MACl produces a shift of the perovskite bandgap from ~1.43 eV, see inset in Fig. 2c, to ~1.55 eV, independently of the method employed to prepare the perovskite film (MWAS or CP) indicating that MA is incorporated into $FAPbI_3$ structure. The blue shift and the ~1.55 eV value agrees well with other values reported into the literature for the $MAFAPbI_3$ [40].

For the preparation of devices, the thin film synthesis temperature of 120 °C was selected as optimal because with this temperature were obtained the best results compared with other synthesis temperatures (100 °C, 110 °C, 120 °C and 150 °C), see Fig. S5. The average performance of $FAPbI_3$ PSCs fabricated with a synthesis temperature of 120 °C is 14.96%, see Fig. S5.

The PCE of PSCs was enhanced adding MACl for devices fabricated with both MWAS $FAPbI_3$ powder and CP solution. The statistics of the $MAFAPbI_3$ photovoltaic parameters are depicted in the Fig. 4. The average solar cell parameters of the devices fabricated with the $MAFAPbI_3$ (MWAS) is 15.29% with an open circuit potential, short circuit current and fill factor of V_{OC}=0.98 V, J_{sc}=22.24 mA/cm^2 and FF=68.5%, respectively. On the other hand, the average parameters for

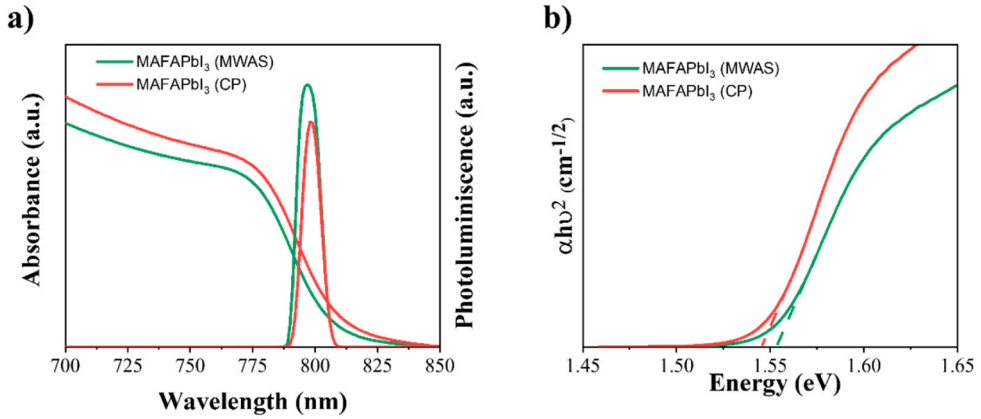

Fig. 3. (a) Absorption and photoluminescence spectra and (b) optical band gap for perovskite films fabricated with the presynthesized $MAFAPbI_3$ powder (labeled as MWAS) and the conventional precursor, FAI and PbI_2, solution (labeled as CP).

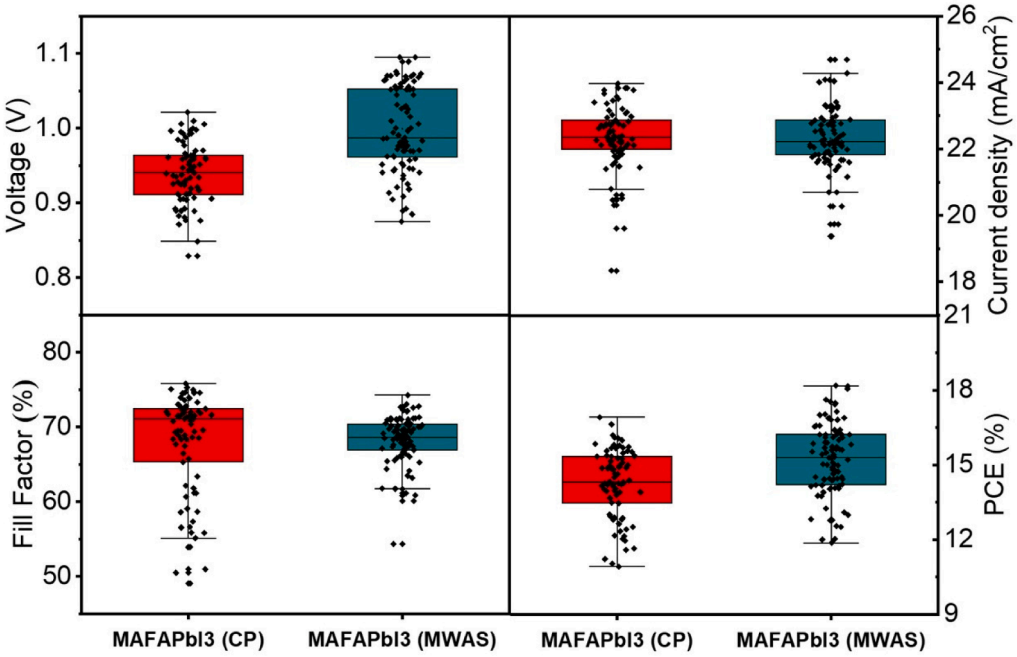

Fig. 4. Statistics have been collected over ten different batches of solar cells fabricated of ≈ 80 $FAPbI_3$ with the conventional precursor solution (CP) and ≈ 90 with the MWAP $FAPbI_3$ powder.

the devices fabricated with the $MAFAPbI_3$ (CP) is 14.31% with an V_{OC}=0.94 V, a J_{sc}=22.35 mA/cm^2 and a FF=71%. The average of these parameters, their dispersion and the parameters for champion devices are summarized in the Table 1. The J-V curves, for the champion devices are shown in the Fig. S6 Note that at less 80 devices from 10 different batches has been prepared in order to have a reliable statistic.

The main advantage of the method presented in this work is the fast way to obtain α-$FAPbI_3$ particles with high crystallinity and low bandgap, which can be stored and easily handled for the preparation of photovoltaic devices by direct dissolution of the ready-to-use powders. However, these results show that the use MWAS $MAFAPbI_3$ powders can produce devices with average (and champion) PCE and Voc higher than the use of conventional precursor solution.

Representative Nyquist plots of electrochemical impedance spectroscopy (EIS) are showed in the Fig. S7 for de CP and MWAS devices. EIS measured were carried out at 0.5 sun, varying the bias voltage from the V_{oc} to 0 V in steps of 0.15 V and varying the frequency from 10^5 Hz (high frequency, HF) to 10^{-1} Hz (low frequency, LF).

Table 1
Summary of the average photovoltaic parameters and the parameters for champion devices (values inside parenthesis) fabricated with $MAFAPbI_3$ as active layer, prepared using both the CP and MWAS $FAPbI_3$ powder.

Name	Voc (V)	Jsc (mA/cm^2)	FF (%)	PCE (%)
MAFAPbI3 (CP)	0.94±0.08 (0.99)	22.4±1.6 (22.61)	71±8 (75)	14.31±1.9 (16.91)
MAFAPbI3 (MWAS)	0.98±0.09 (1.02)	22.0±2.0 (24.69)	68±4 (72)	15.0±2.0 (18.18)

In the Fig. 5a is showed the equivalent circuit used for the IS analysis, as discussed elsewhere [41], containing the series resistance, R_s, associated to the electrodes and wires resistances, the recombination resistance, R_{rec}, considering the transport resistance negligible [41], the geometric capacitance, C_g, as a classical capacitor with electrostatic nature of the films, and parallel branch with a resistance and a capacitance in series, R_{dr} and C_{dr}, accounting for the ionic contributions of the

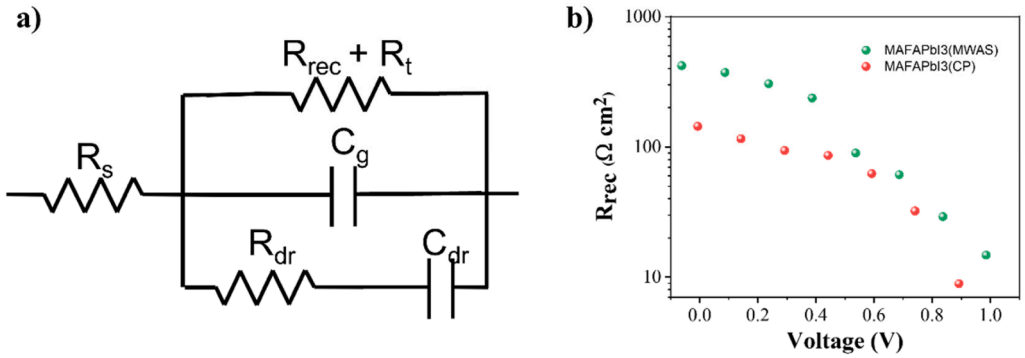

Fig. 5. (a) Equivalent circuit used for the electrochemical impedance spectroscopy analysis [41]. (b) Recombination resistance, R_{rec}, of the MAFAPbI$_3$ MWAS and CP devices.

perovskite film [42].

In the devices fabricated with the MWAS perovskite, the higher V_{oc} is originated by a larger recombination resistance in comparison with the CP devices, see the Fig. 5b, This higher voltage can be produced by the lower recombination rate [43,44] and in line with a low non-radiative recombination [45–47] observed in the PL spectra, see Fig. 3a. In the Fig. S8 the fitted C_g, R_{dr} and C_{dr} values are show. C_g present similar values as expected as the same material films are obtained by both methods. The ionic nature of metal halide perovskites is well accepted [48–51] we can appreciate that samples prepared by MWAS-based solar cells presented higher ionic density, confirmed by the higher C_{dr} and lower R_{dr} [42], respect CP devices, see Fig. S8. This variation would be induced by the different film preparation.

4. Conclusions

To summarize, we demonstrate the α-FAPbI$_3$ powder preparation by microwave-assisted synthesis and its use in perovskite solar cell fabrication. The solar cells fabricated by conventional precursor (CP) solution method and using MWAS powders were compared. The MWAS induce better crystallinity and similar band gap in comparison with the CP solution method. Consequently, devices fabricated from MWAS films present in average higher performance than reference CP solar cells, due to a lower recombination rate as it has been determined by EIS. The addition of MACl has a very positive effect in the films, it produces a δ-phase quasi-free perovskite and grain size bigger that the perovskite without MACl, increasing PCE, but also widening the band gap. The EIS analysis also shows that that MWAS preparation produces higher ion vacancy density films. This work points out the enormous potential of MWAS for applications in perovskite solar cell precursor synthesis.

CRediT authorship contribution statement

Omar E. Solis: Conceptualization, Validation, Writing – original draft. **Carolina Fernández-Saiz:** Conceptualization, Supervision, Writing – original draft. **Jesús Manuel Rivas:** Visualization, Writing – original draft. **Diego Esparza:** Visualization, Writing – original draft. **Silver-Hamill Turren-Cruz:** Conceptualization, Supervision, Writing – original draft. **Beatriz Julián-López:** Conceptualization, Writing – original draft. **Pablo P. Boix:** Writing – original draft. **Iván Mora-Seró:** Conceptualization, Writing – original draft.

Declaration of Competing Interest

The authors declare that they have no known competing financial interests or personal relationships that could have appeared to influence the work reported in this paper.

Data availability

Data will be made available on request.

Acknowledgments

This work is a result of the project STABLE PID2019-107314RB-I00 funded by MCIN/AEI/10.13039/501100011033/ and the European Research Council (ERC) *via* Consolidator Grant (724424 - No-LIMIT). Financial support from COZCyT, UAIE-Universidad Autónoma Zacatecas and Universitat Jaume I (project UJI-B2021-50) is acknowledged. S.H.T.C would like to thank the Spanish Ministry of Economy, Industry and Competitiveness (postdoctoral contract Juan de la Cierva Formación FJC2019-041835-I) for the financial support during this work.

Supplementary materials

Supplementary material associated with this article can be found, in the online version, at doi:10.1016/j.electacta.2022.141701.

References

[1] «Best research-cell efficiency chart». https://www.nrel.gov/pv/cell-efficiency.html (accedido 25 de febrero de 2022).
[2] I.M. De Los Santos, et al., «Optimization of $CH_3NH_3PbI_3$ perovskite solar cells: a theoretical and experimental study», Sol. Energy 199 (2020) 198–205.
[3] W.E. Sha, X. Ren, L. Chen, Y.W.C. Choy, «The efficiency limit of $CH_3NH_3PbI_3$ perovskite solar cells», Appl. Phys. Lett. 106 (22) (2015), 221104.
[4] Q. Wei, W. Zi, Z. Yang, Y.D. Yang, «Photoelectric performance and stability comparison of $MAPbI_3$ and $FAPbI_3$ perovskite solar cells», Sol. Energy 174 (2018) 933–939.
[5] S. Akin, E. Akman, Y.S. Sonmezoglu, «$FAPbI_3$-based perovskite solar cells employing hexyl-based ionic liquid with an efficiency over 20% and excellent long-term stability», Adv. Funct. Mater. 30 (28) (2020), 2002964.
[6] S. Pang, et al., «NH_2CH-NH_2PbI_3: an alternative organolead iodide perovskite sensitizer for mesoscopic solar cells», Chem. Mater. 26 (3) (2014) 1485–1491.
[7] S. Masi, et al., «Chemi-structural stabilization of formamidinium lead iodide perovskite by using embedded quantum dots», ACS Energy Lett. 5 (2) (2020) 418–427.
[8] K.M.M. Salim, et al., «Boosting long-term stability of pure formamidinium perovskite solar cells by ambient air additive assisted fabrication», ACS Energy Lett. 6 (10) (2021) 3511–3521, https://doi.org/10.1021/acsenergylett.1c01311.
[9] S. Masi, A.F. Gualdrón-Reyes, y I. Mora-Sero, «Stabilization of black perovskite phase in $FAPbI_3$ and $CsPbI_3$», ACS Energy Lett. 5 (6) (2020) 1974–1985.
[10] N. Pellet, et al., «Mixed-organic-cation perovskite photovoltaics for enhanced solar-light harvesting», Angew. Chem. 126 (12) (2014) 3215–3221.
[11] M. Salado, S. Kazim, Y.S. Ahmad, «The role of Cs+ inclusion in formamidinium lead triiodide-based perovskite solar cell», Chem. Pap. 72 (7) (2018) 1645–1650.
[12] C. Yi, et al., «Entropic stabilization of mixed A-cation ABX 3 metal halide perovskites for high performance perovskite solar cells», Energy Environ. Sci. 9 (2) (2016) 656–662.
[13] M. Saliba, et al., «Incorporation of rubidium cations into perovskite solar cells improves photovoltaic performance», Science 354 (6309) (2016) 206–209.
[14] S.H. Turren-Cruz, A. Hagfeldt, y M. Saliba, «Methylammonium-free, high-performance, and stable perovskite solar cells on a planar architecture», Science 362 (6413) (2018) 449–453.

[15] M. Saliba, et al., «Cesium-containing triple cation perovskite solar cells: improved stability, reproducibility and high efficiency», Energy Environ. Sci. 9 (6) (2016) 1989–1997.

[16] E.B. Kim, M.S. Akhtar, H.S. Shin, S. Ameen, Y.M.K. Nazeeruddin, «A review on two-dimensional (2D) and 2D-3D multidimensional perovskite solar cells: perovskites structures, stability, and photovoltaic performances», J. Photochem. Photobiol. C Photochem. Rev. 48 (2021), 100405.

[17] J. Rodríguez-Romero, et al., «Widening the 2D/3D perovskite family for efficient and thermal-resistant solar cells by the use of secondary ammonium cations», *ACS* Energy Lett. 5 (4) (2020) 1013–1021.

[18] S. Lv, S. Pang, Y. Zhou, N. Padture, H. Hu, L. Wang, X. Zhou, H. Zhu, L. Zhang, C. Huang, G. Cui, «One-step, solution-processed formamidinium lead trihalide (FAPbI (3−x) Cl x) for mesoscopic perovskite–polymer solar cells», Phys. Chem. Chem. Phys. 16 (2014) 19206–19211, https://doi.org/10.1039/C4CP02113D.

[19] S. Yang, et al., «Thiocyanate assisted performance enhancement of formamidinium based planar perovskite solar cells through a single one-step solution process», J. Mater. Chem. A 4 (24) (2016) 9430–9436.

[20] T. Zhang, et al., «Spontaneous low-temperature crystallization of α-FAPbI3 for highly efficient perovskite solar cells», Sci. Bull. 64 (21) (2019) 1608–1616.

[21] J.W. Lee, Y.N.G. Park, «Two-step deposition method for high-efficiency perovskite solar cells», MRS Bull 40 (8) (2015) 654–659.

[22] J. Duan, et al., «Planar perovskite FAxMA1-xPbI3 solar cell by two-step deposition method in air ambient», Opt. Mater. 85 (2018) 55–60.

[23] J. Du, et al., «Crystallization control of methylammonium-free perovskite in two-step deposited printable triple-mesoscopic solar cells», Sol. RRL 4 (12) (2020), 2000455.

[24] Y. Zhang, et al., «Achieving reproducible and high-efficiency (>21%) perovskite solar cells with a presynthesized $FAPbI_3$ powder», ACS Energy Lett. 5 (2) (2019) 360–366.

[25] M.P. Haris, S. Kazim, y S. Ahmad, «Low-temperature-processed perovskite solar cells fabricated from presynthesized $CsFAPbI_3$ powder», ACS Appl. Energy Mater. 4 (3) (2021) 2600–2606.

[26] G. Tong, et al., «Removal of residual compositions by powder engineering for high efficiency formamidinium-based perovskite solar cells with operation lifetime over 2000 h», Nano Energy 87 (2021), 106152.

[27] A. Leblanc, et al., «Enhanced stability and band gap tuning of α-[HC (NH_2) $_2$] PbI_3 hybrid perovskite by large cation integration», ACS Appl. Mater. Interfaces 11 (23) (2019) 20743–20751.

[28] Y. Zhang, S.G. Kim, D. Lee, H. Shin, Y.N.G. Park, «Bifacial stamping for high efficiency perovskite solar cells», Energy Environ. Sci. 12 (1) (2019) 308–321.

[29] F. Xie, et al., «Vertical recrystallization for highly efficient and stable formamidinium-based inverted-structure perovskite solar cells», Energy Environ. Sci. 10 (9) (2017) 1942–1949.

[30] B. Li, M. Li, C. Fei, G. Cao, y J. Tian, «Colloidal engineering for monolayer CH_3 NH_3 PbI_3 films toward high performance perovskite solar cells», J. Mater. Chem. A 5 (46) (2017) 24168–24177.

[31] A. Brunova, et al., «Structural and trap-state density enhancement in flash infrared annealed perovskite layers», Adv. Mater. Interfaces 8 (14) (2021), 2100355.

[32] S. Dharani, et al., «Incorporation of Cl into sequentially deposited lead halide perovskite films for highly efficient mesoporous solar cells», Nanoscale 6 (22) (2014) 13854–13860.

[33] H. Chen, Y. Chen, T. Zhang, X. Liu, X. Wang, Y.Y. Zhao, «Advances to high-performance black-phase $FAPbI_3$ perovskite for efficient and stable photovoltaics», Small Struct. 2 (5) (2021), 2000130.

[34] M. Kim, et al., «Methylammonium chloride induces intermediate phase stabilization for efficient perovskite solar cells», Joule 3 (9) (2019) 2179–2192.

[35] N. Yantara, et al., «Unravelling the effects of Cl addition in single step $CH_3NH_3PbI_3$ perovskite solar cells», Chem. Mater. 27 (7) (2015) 2309–2314.

[36] T. Zhang, et al., «A facile solvothermal growth of single crystal mixed halide perovskite CH_3 NH_3 Pb (Br 1- x Cl x) 3», Chem. Commun. 51 (37) (2015) 7820–7823.

[37] Z. Wang, et al., «Additive-modulated evolution of HC (NH_2) $_2PbI_3$ black polymorph for mesoscopic perovskite solar cells», Chem. Mater. 27 (20) (2015) 7149–7155.

[38] C. Mu, J. Pan, S. Feng, Q. Li, Y.D. Xu, «Quantitative doping of chlorine in formamidinium lead trihalide ($FAPbI_3$- xClx) for planar heterojunction perovskite solar cells», Adv. Energy Mater. 7 (6) (2017), 1601297.

[39] R.D.J. Oliver, P. Caprioglio, F. Peña-Camargo, L.R.V. Buizza, F. Zu, A.J. Ramadan, S.G. Motti, S. Mahesh, M.M. McCarthy, J.H. Warby, Y.-H. Lin, N. Koch, S. Albrecht, L.M. Herz, M.B. Johnston, D. Neher, M. Stolterfoht, H.J. Snaith, Understanding and suppressing non-radiative losses in methylammonium-free wide-bandgap perovskite solar cells, Energy Environ. Sci. 15 (2022) 714–726.

[40] M.M. Tavakoli, P. Yadav, D. Prochowicz, R. Tavakoli, y M. Saliba, «Multilayer evaporation of $MAFAPbI_3$- xClx for the fabrication of efficient and large-scale device perovskite solar cells», J. Phys. Appl. Phys. 52 (3) (2018), 034005.

[41] S.-M. Yoo, S.J. Yoon, J.A. Anta, H.J. Lee, P.P. Boix, I. Mora-Seró, An equivalent circuit for perovskite solar cell bridging sensitized to thin film architectures, Joule 3 (2019) 2535–2549.

[42] A.J. Riquelme, K. Valadez-Villalobos, P.P. Boix, G. Oskam, I. Mora-Seró, J.A. Anta, Understanding equivalent circuits in perovskite solar cells. Insights from drift-diffusion simulation, Phys. Chem. Chem. Phys. 24 (2022) 15657–15671.

[43] W. Tress, «Perovskite solar cells on the way to their radiative efficiency limit–insights into a success story of high open-circuit voltage and low recombination», Adv. Energy Mater. 7 (14) (2017), 1602358.

[44] M. Yavari, et al., «Reducing surface recombination by a poly (4-vinylpyridine) interlayer in perovskite solar cells with high open-circuit voltage and efficiency», ACS Omega 3 (5) (2018) 5038–5043.

[45] T. Kirchartz, J.A. Márquez, M. Stolterfoht, T. Unold, Photoluminescence-based characterization of halide perovskites for photovoltaics, Adv. Energy Mater. 10 (2020) 1904134.

[46] W. Tress, et al., «Interpretation and evolution of open-circuit voltage, recombination, ideality factor and subgap defect states during reversible light-soaking and irreversible degradation of perovskite solar cells», Energy Environ. Sci. 11 (1) (2018) 151–165.

[47] W. Tress, N. Marinova, O. Inganäs, M.K. Nazeeruddin, S.M. Zakeeruddin, M. Graetzel, Predicting the open-circuit voltage of CH3NH3PbI3Perovskite solar cells using electroluminescence and photovoltaic quantum efficiency spectra: the role of radiative and non-radiative recombination, Adv. Energy Mater. 5 (2015).

[48] Y. Fu, H. Zhu, J. Chen, M.P. Hautzinger, X.-Y. Zhu, y S. Jin, «Metal halide perovskite nanostructures for optoelectronic applications and the study of physical properties», Nat. Rev. Mater. 4 (3) (2019) 169–188.

[49] N. Phung, et al., «The role of grain boundaries on ionic defect migration in metal halide perovskites», Adv. Energy Mater. 10 (20) (2020), 1903735.

[50] Z. Xiao, Y.Y. Yan, «Progress in theoretical study of metal halide perovskite solar cell materials», Adv. Energy Mater. 7 (22) (2017), 1701136.

[51] L. Gu, et al., «Strain engineering of metal–halide perovskites toward efficient photovoltaics: advances and perspectives», Sol. RRL 5 (3) (2021), 2000672.